Investigations of the carbonization process of hybrid polymer microspheres using the TGA-EGA method: assessment of the impact of sulphanilic acid on the process

Magdalena Sobiesiak[1] · Beata Podkościelna[1] · Liliana Mazur[2]

Abstract

The TGA-EGA technique was used to study the influence of sulphanilic acid (SA) on the carbonisation process of the hybrid terpolymeric precursors composed of methacrylamide, divinylbenzene, and trimethoxyvinylsilane. The pristine polymers were impregnated with saturated solution of SA, dried, and carbonized at 600 °C under N_2 atmosphere. The characteristic properties of both the pristine hybrid polymers and the resulting carbons were based on FTIR, Raman, and PXRD analyses, which revealed the materials were composed of amorphous polymeric or carbon phase interpenetrated by silica/silicate disordered network. The porosimetric analysis showed the resulted carbons possessed homogeneous supermicropores with the average pore width of 0.7 nm and reduced number of mesopores compared to pristine precursors. From the TGA results, it was followed that impregnated polymers decomposed in two stages, instead of one like pristine precursors did. Moreover, IDT of impregnated polymers was reduced by about 100 °C, and their T_{max} was increased by 2–5.5 °C. Their decomposition proceeded slower by 22–37% that caused increase in efficiency of the process by 10–48%. The EGA showed the decomposition of the impregnated precursors started from the degradation of the amide groups, then SA destruction took place, followed by further decomposition of the polymer. The studies led to the conclusion that SA had the protective effect on the surface of the carbonized polymers. During impregnation and thermal treatment, SA produced a deposit in pores of the precursors. This resulted in narrowing of the pore width, delaying and slowing down the polymer thermal decomposition process, as well as increasing its efficiency.

Keywords Hybrid materials · Hybrid polymers · Hybrid carbons · TGA-EGA · Carbonisation · Sulphanilic acid

Introduction

Hybrid polymer materials are of great interest nowadays. In their structure, they combine polymer chains with inorganic molecules, allowing to obtain new products with improved or even unique properties, e.g. thermal, mechanical, rheological, electrical, catalytic, fire retardancy, or optical [1–5]. These modern materials can be used in various, sometimes very distant, fields, such as medicine, cosmetics, textiles, agriculture, food packaging, catalysis, construction, optics, and optoelectronic devices, as well as in very advanced technologies for semiconductor devices, sensors, or aerospace [1, 6]. When prepared in the form of porous microspheres, they can be efficient adsorbents used in purification and separation techniques [7, 8]. They can also be a substrate for the synthesis of hybrid porous carbons, which have a much higher chemical and thermal resistance than their polymer precursors [9–11].

Depending on a way of synthesis and used substrates, especially the one that contributes the silica-derivative component, the obtained hybrid and composite materials may significantly differ from each other in terms of structural properties. Silica or silicate species can create varied forms ranging from completely disordered and amorphous [12, 13], through partially ordered (composed of defective octamers or ladder-like fragments [14, 15]), to crystalline [16, 17] or channel-like highly ordered [3, 18]. Their rigid structure not

✉ Magdalena Sobiesiak
magdalena.sobiesiak@umcs.pl

[1] Department of Polymer Chemistry, Faculty of Chemistry, Maria Curie-Sklodowska University, Pl. Marii Curie-Sklodowskiej 5, 20-031 Lublin, Poland

[2] Department of General and Coordination Chemistry, Faculty of Chemistry, Maria Curie-Sklodowska University, Pl. Marii Curie-Sklodowskiej 5, 20-031 Lublin, Poland

only allows to construct internal three-dimensional frameworks, which constitute an element reinforcing the material [19], but also influences its thermochemical and insulation properties contributing to the increase in thermal and fire resistance [4, 5, 9, 20]. According to the literature reports, a decomposition of hybrid or composite polymeric materials begins from organic parts, especially linear aliphatic hydrocarbon chains, whilst Si–O-containing species are incorporated into arising SiO_xC_y network. Although the formation of such cross-linked structure prevents further destruction of the material, around 600 °C, its density increases, indicating a continuous reorganisation of the structure towards an inorganic silica-like phase that forms a protective barrier on the surface even at higher temperatures [21–24].

The second factor that contributes to the improvement of the thermal properties of polymers and gives them flame resistance and the ability to self-extinguish is the presence of nitrogen atoms in the polymer chain [11]. Synthetic polymers such as polyamides, polyimides, poly (meth)acrylamides, or polyacrylonitriles, as well as natural ones, e.g. chitosan, are popular precursors used in the synthesis of carbon materials [24–28]. Studies on pyrolysis of various nitrogen-containing polymers have shown that, regardless of the type of used precursor, there are four main N-derivative functional groups in the charred matter: pyridinic, pyrrolic/pyridone, graphitic (quaternary) N, and N-oxides [29–33]. Thermogravimetric analyses performed on samples polymethacrylimides and polyacrylamides revealed that below 340 °C, pendant amide groups condense to form imides with the release of ammonia as a by-product. Above this temperature, intensive mass loss occurs as a result of the breakdown of the main polymer chains. This process is accompanied by the emission of water, carbon dioxide, imides, and nitrile compounds. In the general course of thermal degradation, the imidisation and dehydration reactions of amide groups and radical decomposition of the polymer chains with inter- and intramolecular hydrogen transfer take place [34, 35]. The process is complex and assisted by many side reactions in which gaseous decomposition products can still react with the carbonaceous material. Consequently, the formation of the nitrogen-containing functional groups mentioned above occurs. These moieties are responsible for carbon characteristic features such as polarity or acid–base properties of its surface, resulting from their concentration and chemical heterogeneity. It makes that nitrogen-doped carbonaceous materials find applications in heterogeneous catalysis, adsorption, and as components of batteries or carbon electrodes [32].

Zuo et al. tested properties of polyimide films casted on soda glass. They found that the polarity of the polyamide films carbonized up to 300 °C on the glass side was higher than that on the air side. The observed phenomenon was explained by the presence of hydrogen bonds between the polar groups of the polymer and the silanol groups of the glass, which they believed were to prevent imidisation [26]. This observation seems to be useful in the field of synthesis of hybrid and composite materials, because it indicates the formation of quite strong interactions between the functional groups of the polymer and the inorganic silica/silicate framework. Due to their presence, structures with a low degree of order may be formed in the amorphous network of the hybrid material.

Another extremely important factor required in potential applications of hybrid materials is a uniform porous structure. In the case of polymers, the porosity is created already on an early stage of a synthesis by, e.g. control of cross-linking degree [36], using appropriate porogenic solvents [37, 38] or hybrid monomer [7] or template [39]. The formation of the porous structure of carbon materials depends on the technique of their synthesis. In classical carbonisation, the porosity of precursor and the conditions of the process are extremely important as they affect the porous properties of the final carbon product [40, 41]. One of the drawbacks of this method is relatively low possibility to control the width of the pores. In order to overcome this inconvenience, additional procedure involving chemical vapour deposition (CVD) can be applied [42–45]. An alternative way to achieve carefully planned and designed porosity of carbons is template techniques. They allow to obtain carbons with desired type of pores by choosing the right template substrate [46–49]. The materials prepared with these methods have uniform, well defined, and even hierarchical pores, which can form, e.g. interconnected channels [50, 51]. Similar results can be obtained by carbonisation of hybrid polymeric precursors [11].

In this work, we present the application of thermogravimetry with the analysis of evolved gases (TGA-EGA) to study the course of the carbonisation process of porous hybrid polymer microspheres impregnated with sulphanilic acid as a surface modifier supporting the control of pore width. Sulphanilic acid has not yet been tested as such type of agent, but its potential seems to be very interesting. This simple compound decomposes, releasing sulphur dioxide and aniline. The former can act as a gas activating the carbon surface, whilst the latter, depositing in the porous structure, makes it more uniform, similarly to the CVD method. Moreover, one of the advantages of the impregnation procedure is the consumption of a much smaller amount of reagent compared to the CVD.

TG analyses revealed that thermal decomposition of the pristine hybrid polymers started in the range of 240–350 °C with higher values being achieved by samples with higher trimethoxyvinylsilane (TMVS) content, whilst the impregnated ones were much less thermally stable, and their initial decomposition temperature was shifted to the range of 177–211 °C. Also, the course of the decomposition was significantly different. In case of the former, it was a fast

one-stage process (peak around 447 °C), whilst for the latter, it ran in two slower steps (334 and 449 °C).

Evolved gas analysis of methacrylamide–divinylbenzene copolymer (HPP 1) revealed compounds characteristic of polymers of this type, mainly ammonia, unsaturated hydrocarbons, CO_2, amide, and imide species. As the content of TMVS in polymers increased, the proportion of ammonia derivatives decreases, whilst aromatic compounds, e.g. aliphatic styrene, derivatives predominated. In case of the impregnated polymers, at the first stage of the polymer decomposition, besides ammonia, SO_2 was also released. Then at the beginning of the second stage, mainly aniline was evolved, but as the process progressed, other hydrocarbon components, originating from DVB mers, appeared in the decomposition products too. At the final stage, methane and increasing amounts of CO_2 were recorded, as well. This observation suggested that at this stage, the polymer was already carbonized and further structural changes resulted from the internal transformation of this newly formed charred matter. The conducted experiments showed that the modifier was completely decomposed, and the products of its decomposition contributed to the formation of both the porous structure and the chemical heterogeneity of the surface of carbon products.

Experimental

Materials—reagents

Sulphanilic acid of analytical grade and methanol and acetone of pure grade were purchased from POCH (Gliwice, Poland). Highly purified water of Millipore quality was prepared in our laboratory using Synergy® Water Purification System, Millipore (Merck).

Materials—preparation of the samples

The hybrid polymeric porous precursors (HPP) in form of microspheres were synthesized using methacrylamide (MA) as the primary monomer, divinylbenzene (DVB) as crosslinking monomer, and trimethoxyvinylsilane (TMVS) as a source of inorganic framework of the hybrid polymer. The obtained polymers differed in the content of the monomers molar ratio: HPP 1–MA-DVB-TMVS (2:1:0), HPP 3–MA-DVB-TMVS (1.33:1:0.67), HPP 4–MA-DVB- TMVS (1.5:1:0.5), and HPP 6–MA-DVB-TMVS (0:1:1). All the details regarding the syntheses of precursors were already described in previous work [52].

In order to obtain a more homogeneous porous structure of the final carbonisation products and support a process of thermal treatment, the resulting polymers were impregnated with sulphanilic acid (SA). The impregnation was carried out with a saturated aqueous solution of SA using 10 mL for each 1 g of the polymer precursor. Next, the samples were dried and carbonized at 600 °C under nitrogen atmosphere (100 mL min^{-1}) to obtain hybrid porous carbons (HPC). After carbonisation, all the materials were washed with methanol and acetone in Soxhlet apparatus for at least 8 h and left to dry. The numbers on the HPC labels indicate the corresponding polymer precursor.

Measurements

Porous structure analysis

Porous structure parameters were evaluated using standard low-temperature nitrogen sorption experiments performed with an ASAP 2405 analyser (Accelerated Surface Area and Porosimetry system, Micromeritics Inc., Norcross, GA, USA). Before analyses, the samples were outgassed at 70 °C for 1 h. The adsorption–desorption isotherms were measured at − 196 °C. The specific surface area (S_{BET}) was calculated using the standard BET method assuming N_2 molecular cross-sectional area of 0.162 nm. The total pore volume (V_{tot}), mesopore and micropore volumes, and pore size distributions were calculated by means of SAIEUS software (Micromeritics), free version, www.nldft.com, choosing the implemented 2D-NLDFT model. The performed calculations were based on adsorption branch of the isotherms and the heterogeneous pore model.

Attenuated total reflectance spectroscopy

Infrared spectra were collected in Attenuated Total Reflectance mode (ATR-FTIR) by means of a TENSOR 27 spectrophotometer (Bruker, Ettlingen, Germany). The spectra were acquired in the frequency range of 4000 to 600 cm^{-1} at a resolution 4 cm^{-1}, performing 32 scans per measurement. For processing, the collected data from OPUS software (provided by the equipment manufacturer) were applied. The resulting spectra were shown as a function of transmittance versus wavenumber.

Raman spectroscopy

Raman spectra were recorded with the use of a Renishaw inVia Reflex Raman microscope, wavelength of excitation laser was 514 nm, and its power was about 1.4 mW. One spectrum, with a resolution of 1 cm^{-1}, was recorded per measurement. These spectra also were processed with OPUS software.

Powder X-ray diffraction measurements

The powder X-ray diffraction (PXRD) data were collected with the PANalytical Empyrean diffractometer with Ni-filtered Cu Kα radiation (Malvern PANalytical, Malvern, UK). The measurements were taken at room temperature. The intensity data were captured with the PIXcel3D detector over the 2θ range of 5–50° with the step of $\Delta\theta = 0.013°$. The overlays of diffraction patterns were generated using HighScore software.

Thermogravimetric analysis coupled with infrared spectroscopy of evolved gases

TG/DTG analyses were carried out using an STA 449 F1 Jupiter thermal analyzer (Netzsch, Selb, Germany). Samples of approximately 7 mg were weighed into a Al_2O_3 crucible. Measurements were taken in the range of temperature from 30 to 1000 °C with the heating rate set on 10 °C min^{-1}. During analyses, helium atmosphere was maintained with a flow rate of 40 mL min^{-1}. The gaseous products evolved (EGA) from the heated sample were analysed with the online coupled Fourier transform infrared spectrometer FTIR Tensor 27 (Bruker, Ettlingen, Germany). Similar to ATR measurements, these spectra were collected in the same frequency range and resolution; however, 16 scans were recorded per sample scan time. To distinguish EGA spectra from those of ATR, the former was shown in absorbance units (A.U.). The interpretation of the collected spectra included both analysis of the most characteristic, individual vibration bands using correlation tables and comparison of the obtained results with reference spectra for substances in the gaseous state, which are available in the NIST database.
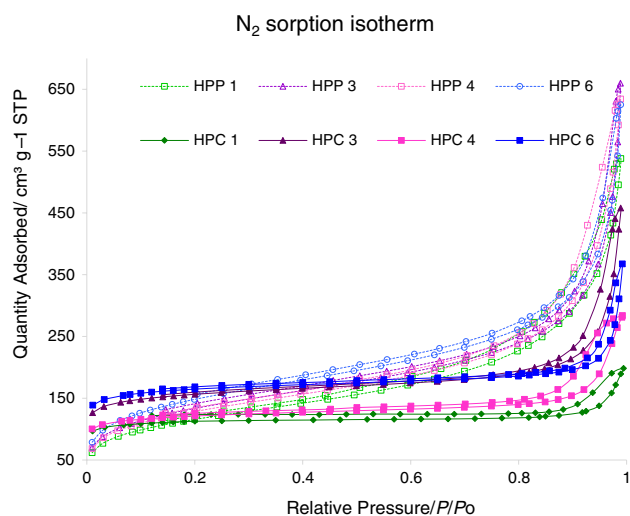

Fig. 1 N_2 adsorption–desorption isotherms of polymer precursors and the carbons obtained out of them

Results and discussion

Porosity

The effect of using sulphanilic acid as a substance modifying the surface properties of the precursor materials is at first revealed in the results of porosimetric analysis (Table 1). Although specific surface areas (S_{BET}) did not change significantly when comparing their values between the respective polymer precursor and its carbonisation product, the total pore volumes (V_{tot}) were reduced by 32 even to 63%. However, it did not imply deterioration or loss of the material porosity, since the micropore volumes (V_{mi}) increased about 10 times in all cases. This was associated with a decrease in the average pore size (W) by about 50%.

The above-described structural changes are especially well visible in plots presenting nitrogen sorption isotherms (Fig. 1) and pore size distributions (PSD) (Fig. 2). All the hybrid polymers possessed very uniform, almost identical mesoporous structure with dominating pores of 22 nm width. Only up to 2% of the total pore volume was micropores. They had mean pore width of ca. 1.2 nm. After carbonisation, percentage contents of the smallest pores became much higher and reached even up to 45%. The average widths were shifted to the value of ca. 0.7 nm, which is characteristic of supermicropores. Their presence is represented by very sharp and narrow peaks in Fig. 2. Some changes were also observed in the region of mesopores. The volume of mesopores in range of 5–30 nm was significantly reduced, whilst those of 2–5 nm almost totally disappeared. In case of HPC 6, additional effect is observed, as in the range of 10–30 nm, only one wide peak could be observed that proved the structural transformation affected to a greater
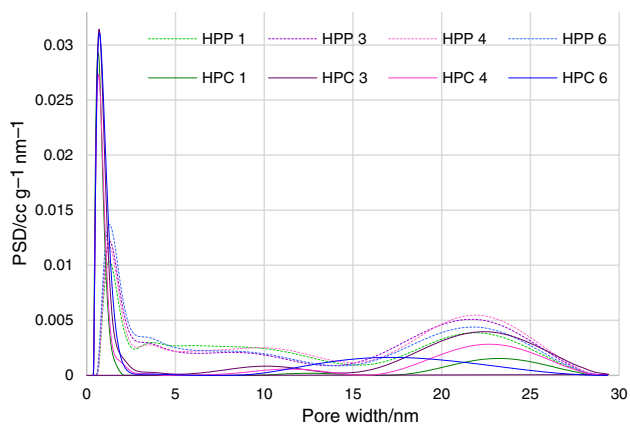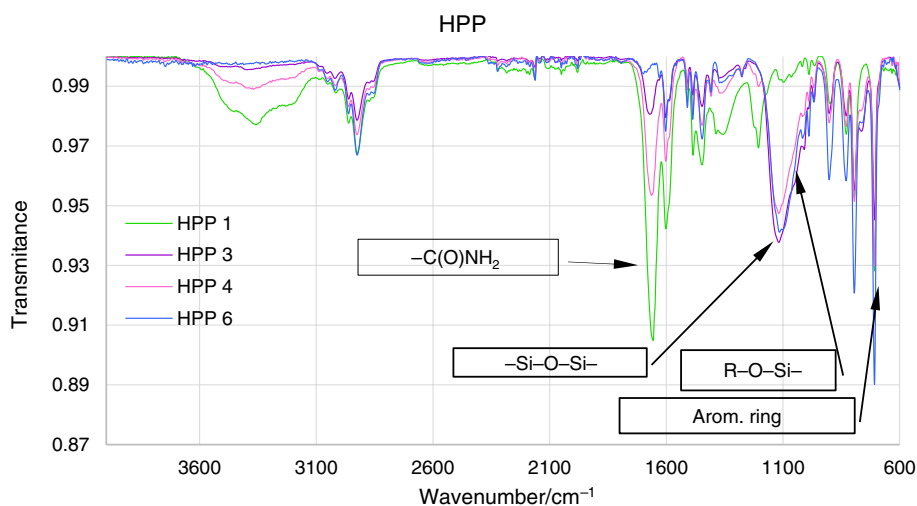
Table 1 Porous structure parameters of the hybrid polymeric precursors and the hybrid carbons

Material	$S_{BET}/$ m^2 g^{-1}	$V_{tot}/$ cm^3 g^{-1}	$V_{mi}/$ cm^3 g^{-1}	Percentage of micropores/%	W/nm
HPP 1	400	0.83	0.015	1.81	8.0
HPP 3	461	1.05	0.016	1.52	8.5
HPP 4	443	0.98	0.017	1.73	8.5
HPP 6	511	0.97	0.019	1.96	7.3
HPC 1	400	0.31	0.14	45.16	3.2
HPC 3	553	0.71	0.16	22.54	5.2
HPC 4	430	0.44	0.14	31.82	4.2
HPC 6	584	0.57	0.19	33.33	4.0

Fig. 2 Pore size distribution plots of the studied materials

Fig. 3 ATR spectra of hybrid polymer precursors HPP 1– HPP 6

latter includes, for example, partial hydrolysis and condensation of TMVS leading to the formation of hydroxyl (at 1020–1040 cm^{-1}) and silicate species (at 860–1180 cm^{-1}) [13]. In this region, asymmetric vibrations of Si–O–Si cyclic structures can be found at 1118 cm^{-1} [54], as well. Additionally, the possibility of bond formation with aromatic rings should also be considered. The strongest characteristic vibrations of Si–O–C(sp^2) and Si–C(sp^2) are in the ranges of 1090–1135 and 1090–125 cm^{-1} [55], respectively.

After carbonisation, the bands of Si–O–C and Si–O–Si become dominating; however, their position is a little shifted towards lower values of wavenumbers just under 1100 cm^{-1} (Fig. 4). The aromatic ring vibrations still can be observed at about 1600 and 800 cm^{-1}, but their shapes are different than in case of the polymers. It is a consequence of characteristic

extent larger pores, leading to a narrowing of their widths. However, the almost complete disappearance of mesopores narrower than 10 nm may indicate that the process of pore merging also took place.

Spectral analysis

ATR-FTIR spectra presented in Fig. 3 confirm the chemical structures of the hybrid polymeric precursors. At about 1657 cm^{-1}, vibrations of amide groups can be observed. From the right at 1600 cm^{-1}, a band coming from DVB aromatic system is superimposed on them. However, the most intense bands of aromatic rings can be found below 830 cm^{-1}. In the range of 970–1180 cm^{-1}, there are medium-intensity bands originating from silicone-containing species [53]. These bands are a combination of primary vibrations of TMVS functionalities: asymmetric stretching of Si–O–C in CH$_3$–O–Si (at 1000–1110 cm^{-1}) and Si–CH– (at 1000–1020 cm^{-1}), as well as secondary vibrations of moieties formed during polymerisation and in side reactions. The

structure of carbon materials formed by different-size disordered clusters of condensed and defective aromatic species. The absence of amide band proves that these moieties had decomposed during heat treatment.

In Raman spectra of the precursors (Fig. 5), mainly bands from hydrophobic parts of the polymers are well visible. The most intense of them is caused by vibrations of aromatic system of DVB monomer. They include number of peaks in the range of 3100–3000 cm^{-1} due to stretching of =C(sp^2)–H, stretching of aromatic rings at about 1600 cm^{-1}, and that at about 1000 cm^{-1} indicating the ring substitution positions. The another mid-intensity band located between 3000 and 2840 cm^{-1} reflects the presence of C–H bonds in longer fragments of the aliphatic chains and shorter linkages cross-linking adjacent chains [55].

The Raman spectra of the carbons (Fig. 6) have shapes typical of carbonized materials. The highest intensity possesses G bands at about 1600 cm^{-1} representing vibrational modes of asymmetric stretch of sp^2 carbons. At

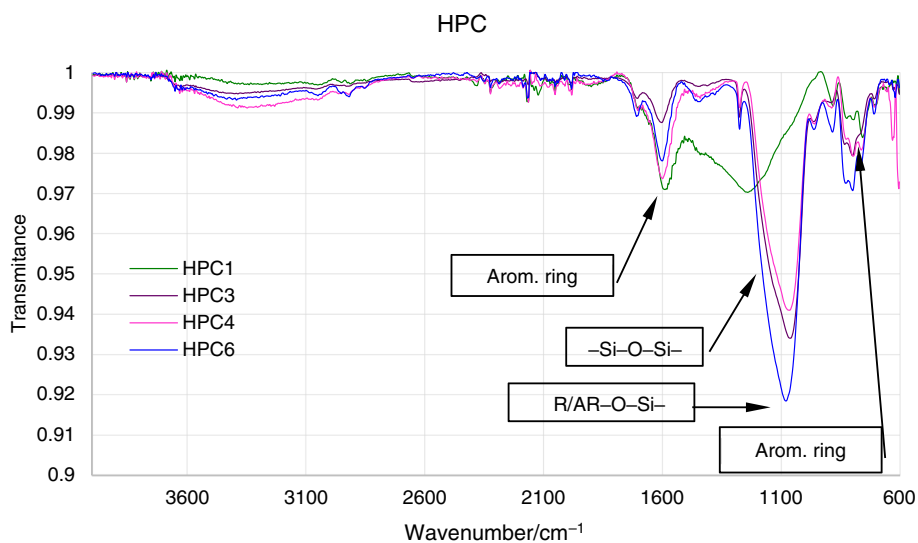**Fig. 4** ATR spectra of hybrid porous carbons HPC 1–HPC 6

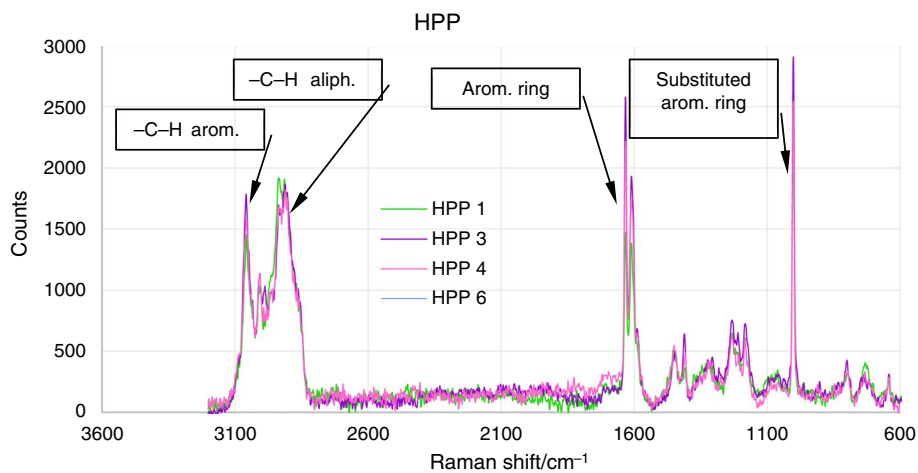**Fig. 5** Raman spectra of hybrid polymer precursors HPP 1–HPP 6

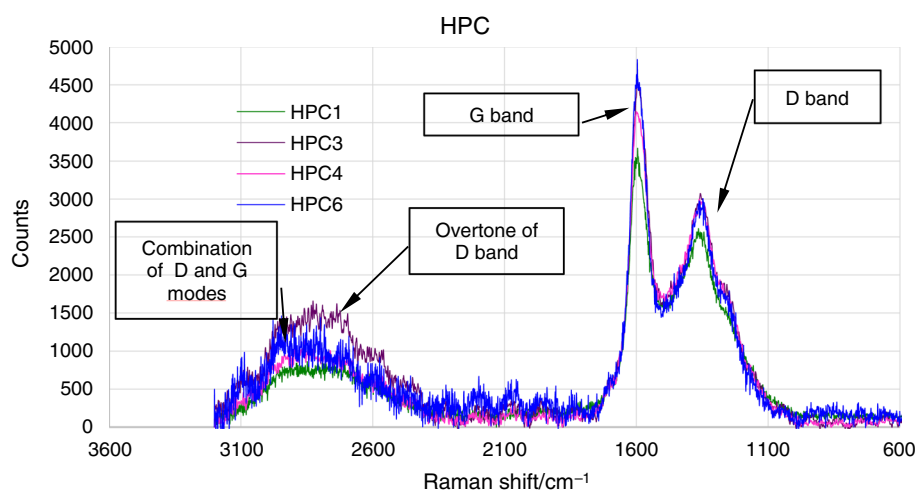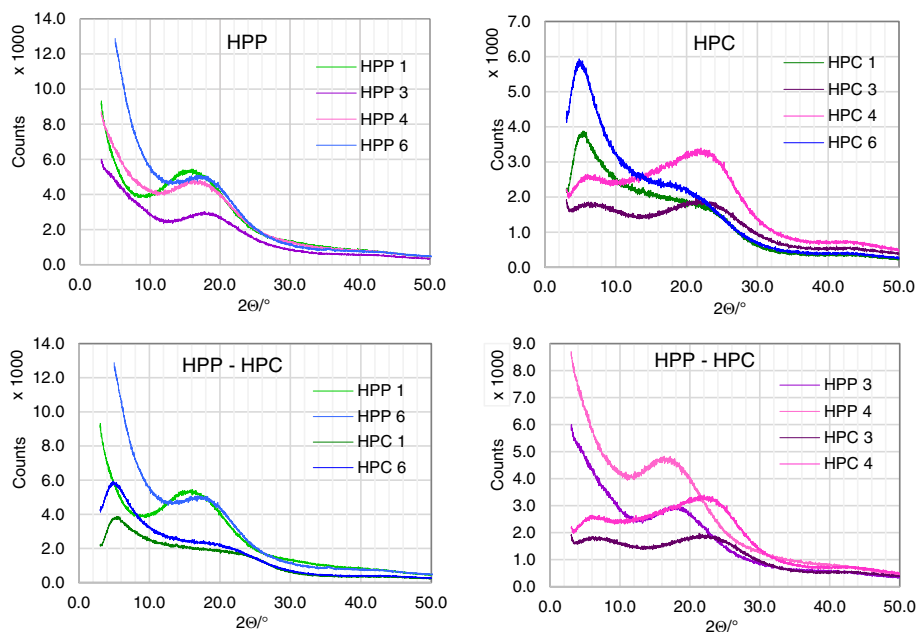**Fig. 6** Raman spectra of hybrid porous carbons HPC 1–HPC 6

Fig. 7 The PXRD patterns of the HPP and HPC samples

ca. 1350 cm^{-1}, D bands are visible as broad peaks of medium intensity. They are assigned to symmetric breathing modes and Kekule-type vibrations in larger ring systems [56]. In the range of 3100–2400 cm^{-1}, s-order vibration bands are active giving very broad peak consisting of combination of D and G modes (at ca. 2900 cm^{-1}) and D bands overtones (at about 2700, 3100, and 2400) [57].

The obtained Raman spectra are very similar to each other, which proves that for all the precursors, the course of formation of the carbon structure proceeded in a comparable manner.

PXRD analysis

The powder patterns of HPP and HPC materials are shown in Fig. 7. For better exposition of the structural differences between the tested samples, the comparisons of the results obtained for polymers (HPP; on the left) and carbons (HPC; on the right) are presented in the upper panel, whereas the bottom panel allows to confront the results for individual pairs of the polymer precursors and the carbons obtained from them, in order to better estimate the structural changes occurring under carbonisation conditions.

The PXRD studies revealed that all the analysed samples were amorphous. In the patterns, three regions can be distinguished in the ranges of 5–10°, 10–30°, and above 30°, respectively. Broad diffraction peaks in these regions occur for polymers, carbons, and silica materials.

In case of amorphous polymers, two broad diffraction peaks extending between 10–15° and 15–24° are assigned to two different amorphous phases associated with the orientation and length of two adjacent polymeric chains [58]. For

polystyrene (PS), the peaks are observed at 10° and 19° corresponding to the interchain and intrachain distances, respectively, caused by phenyl–phenyl interchain and phenyl–chain interactions [59, 60]. When amide groups are present in polymer, the characteristic positions of the reflections are ca. 21° and 22.6°. The former is assigned to the average distance between H-bonded chains, whilst the latter to the average van der Waals distance between the non-H-bonded chains [59, 61]. The presence of the side chains is also affected in the PXRD patterns. Their steric hindrance influences the distance between polymer chains, and the more bulky the side chains are, the greater the distance between the chains will be created. This, in turn, is not conducive to the formation of structures with a higher crystalline/spatial order [59, 61]. On the other hand, if a polymer has the ability to form lamellar structures in the range of lower-angle reflections (below 10°), broad peaks are present. They are attributed to lamella stacking distance [62].

Hung et al. studied poly(divinylbenzene) (PDVB) microspheres and its carbonized derivatives [63]. In the PXRD pattern of PDVB, one broad reflection located at about 18° was found. After carbonisation, the peak position changed to ca. 23°, and a new one appeared at about 43°. Both of them were assigned to the largely disordered carbon. Similar peaks were also observed in PXRD patterns of other carbonized materials prepared from different sources including those of natural origin [64, 65]. The above-mentioned reflections correspond to (002) and (100) planes of graphite, respectively. According to structural and theoretical studies [64, 66], the presence of the former is due to a small number of stacked graphene layers, which are more distant from each other than in graphite (3.35 Å), whilst the latter (43°)

Fig. 8 The TG (left) and DTG (right) curves of the pristine HPP samples
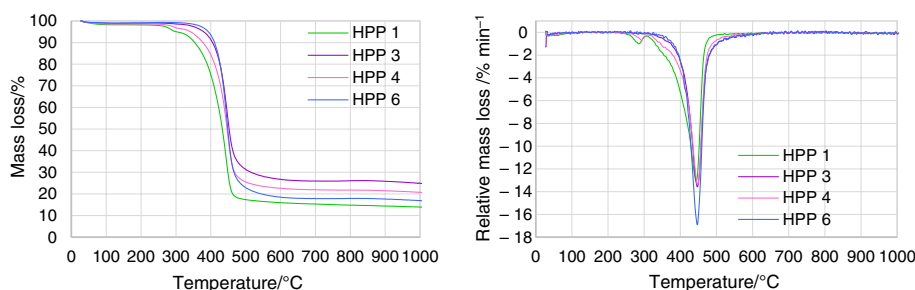
is attributed to the dimension of the average crystallite in the in-plane direction. The factors influencing the position and width of the diffraction reflections (broadening of the finite size of crystals, parameter fluctuations, and lattice deformations) include the source of carbon, the method of its preparation, and chemical treatment [64]. In the case of carbons prepared at the temperatures below 1000 °C, the reflections are broad, and their intensities are small, indicating a heavily disordered structure with very little crystallinity covering only small graphene-like fragments stacked of average two layers [63, 65, 67, 68].

The literature reports prove that also silicate species possess their reflections in the above-mentioned ranges [14–16, 21]. The reflections below 14° are attributed to fourfold siloxane rings originating from the cyclic structures arranged in the macromolecular network of silicates, whilst those located in range 14–30° to amorphous silica.

As follows from Fig. 7, for the HPP samples, each polymer has only one peak visible in the range of 8–30°. Its position and width change slightly depending on the polymer compositions. The broadest (8–30°) peak with a maximum at ca. 16° was obtained for HPP 1 composed of methacrylamide and divinylbenzene. In the case of HPP 3, HPP 4, and HPP 6, the reflections became narrower and shifted towards 18° with the increasing content of trimethoxyvinylsilane monomer in the polymer.

The PXRD patterns of the HPC samples have reflections in the areas characteristic of carbon materials (ca. 23 and 43°), and their profiles are typical of those with highly disordered structure. In analogy to the HPP, the broadest and least intense peaks were for HPC 1. Very similar results were

obtained for HPC 6 proving that both materials retained the amorphous structure of their precursors to great extent. This is also confirmed by the presence of strong amorphous phase diffusion observed for low 2Θ angles. A slightly higher order of the carbon structure was exhibited by HPC 3 and HPC 4. These two samples had better developed peak at 23°; at the same time, that at 43° was almost unchanged. This observation can lead to the conclusion that all the HPCs are built of very small fragments resembling randomly arranged polycyclic aromatic hydrocarbons (PAHs) of various sizes rather than graphene crystallites. However, in the case of HPC 3 and HPC 4, the presence of broad but more intense reflection at 23°can indicate the beginning of the stacking process.

Taking into account the structural changes in polymers caused by carbonisation (bottom panel of Fig. 7), the reflections not only shifted from about 16–18° for HPP to 23° for HPCs, but also their intensities decreased, which was especially pronounced for HPC 1 and HPC 6. The shift is a consequence of reducing the distance between polymer chains, which takes place when the processes of their cyclisation and aromatisation occur during the formation of the carbon structure. It is well-known that even in amorphous phase, short fragments of polymer chains can be parallel to each other due to, e.g. van der Waals, interactions. These areas are destroyed during carbonisation, resulting in the intensity reduction of reflections.

Thermal properties

The effect of chemical composition of the pristine hybrid polymers precursors on their thermal properties is presented

Table 2 Thermal parameters of the pristine hybrid polymeric precursors

	IDT/°C	$T_{10\%}$/°C	$T_{25\%}$/°C	$T_{50\%}$/°C	DT/°C	Δm/%	Rm/%	T_{max1}/°C	Rate of 1st stage/% min^{-1}	T_{max2}/°C	Rate of 2nd stage/% min^{-1}
HPP 1	260.8 2.3%	353.8	400.3	433.0	400.9–458.9	68.57	13,38	284.3	1.04	444.4	13.17
HPP 3	299.9 1.3%	406.0	432.3	452.4	417.5–466.0	64.03	23.90	–	–	447.1	13.79
HPP 4	264.6 1.8%	377.4	419.9	446.2	411.9–464.2	63.54	20.45	293.2	0.69	447.2	13.35
HPP 6	332.0 1.1%	411.0	431.7	448.5	420.1–464.8	71.56	16.20	–	–	446.9	16.91

Fig. 9 The TG (left) and DTG (right) curves of the impregnated HPP samples
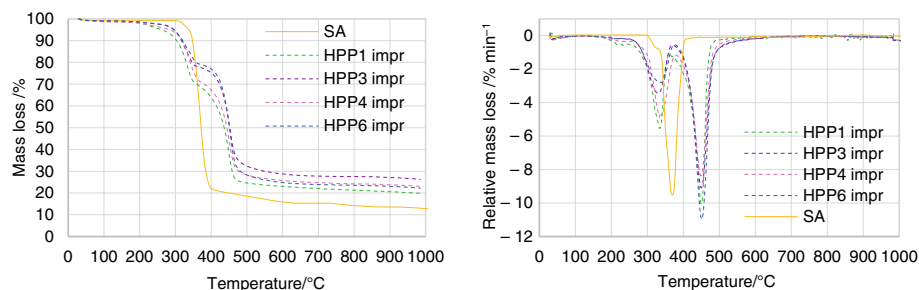
in Fig. 8 and Table 2. In order to compare thermal stability of the studied materials, the temperatures corresponding to 10, 25, and 50% of sample mass loss ($T_{10\%}$, $T_{25\%}$, and $T_{50\%}$) for the polymers and 5, 10, and 20% ($T_{5\%}$, $T_{10\%}$, and $T_{20\%}$) for the carbons were determined from the TG curves. Additionally, the initial decomposition temperature (IDT) of polymers and the full range of sample decomposition temperature (TD) were estimated. From the point of view of carbonisation efficiency, the residual mass (Rm) and the sample mass change (Δm) within the decomposition range or to a given temperature range are also important parameters. The temperature of the maximum decomposition rate (T_{max}) and the rate of decomposition were determined from the DTG curves for each stage of the process.

TG analyses revealed that thermal decomposition of the pristine polymers started in the range of 260–330 °C, and values of IDT and $T_{10\%}$ strongly depended on the contents of methacrylic component in the sample. At the beginning of decomposition of HPPs containing higher amounts of MA (HPP 1 and HPP 4), a slight and slow mass change was observed in the range of 250–300 °C. In case of HPP 3, it was hardly visible, and for HPP 6, it was absent at all. This observation indicated that the thermal degradation of the polymers began with the MA component. At higher decomposition temperatures ($T_{25\%}$ and $T_{50\%}$), another trend is more pronounced. The increase in the TMVS monomer content contributed not only to the improvement of the thermal stability of the polymers but also, due to smaller mass changes (Δm), allowed to obtain higher residual masses. Interestingly, this effect was most pronounced for HPP 3 and HPP 4, confirming a synergistic

stabilisation of the structure by each component of the polymer. For this reason, the highest efficiencies of carbonisation, exceeding 20%, were achieved just for these two polymers [23].

Based on the DTG analysis results, it was found that for all samples containing TMVS, the temperatures of maximum decomposition rates were almost identical ~447 °C and with the decreasing contents of MA, the process proceeded in one stage, but with a higher rate. It means that, although MA contributed to lowering the IDT of polymers, the carbon structure formed from it decomposed more slowly than that of the highly cross-linked DVB (HPP 6). This finding is in line with results reported in the literature [24, 26, 34, 35].

The influence of sulphanilic acid on the thermal behaviour of polymers after impregnation is shown in Fig. 9, and relevant data are collected in Table 3. For comparison, the results for pure SA have also been added. It is worth noting that IDT of SA is very high due to its zwitterionic crystal structure additionally supported by hydrogen bonds between amino and sulphonic groups [69].

The impregnated polymers were much less thermally stable, as their decomposition started in the range of 177–211 °C, which was about 60–100 °C lower than for the pristine precursors. The reason of this phenomenon was that SA in narrow pores of HPPs could not form stable crystal structure, which consequently led to a decrease in its thermal stability. As the result, the ranges of DT were slightly extended. Moreover, the course of the decomposition was significantly different. In this case, it proceeded in two slower but clearly marked stages (T_{max1} ~ 334 and T_{max2} ~ 449 °C).

Table 3 Thermal parameters of the impregnated hybrid polymeric precursors and sulphanilic acid

	$IDT_{1.5\%}$/°C	$T_{10\%}$/°C	$T_{25\%}$/°C	$T_{50\%}$/°C	DT/°C	Δm/%	Rm/%	T_{max1}/°C	Rate of 1st stage% min^{-1}	T_{max2}/°C	Rate of 2nd stage% min^{-1}
HPP 1 impr	177.2	303.4	339.5	436.3	386.9–465.0	72.06	19.87	334.1	5.55	449.9	10.07
HPP 3 impr	195.8	316.8	401.8	451.8	404.8–470.4	65.02	26.31	330.1	3.46	449.9	9.09
HPP 4 impr	159.9	320.3	352.5	443.8	390.0–470.0	67.43	22.99	333.8	4.87	449.2	8.39
HPP 6 impr	211.3	319.7	412.5	451.3	412.0–470.4	69.56	22.29	338.2	2.81	450.9	10.97
SA	352.0	362.7	367.0	377.7	340.0–390.0	75.4	12.1	341.0	3.20	371.0	19.84

Fig. 10 The TG (left) and DTG (right) curves of the HPC samples
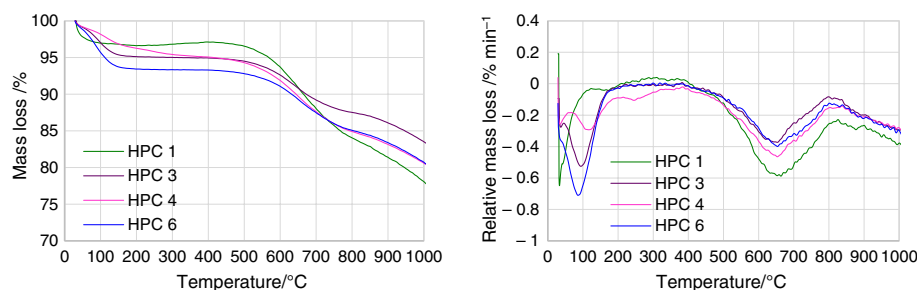
Taking into account the second stage of decomposition and comparing T_{max2} for HPP and HPP impr polymers, it should be stated that after impregnation, the obtained values were 2–5.5 °C higher. Similar comparison made for decomposition rates allowed to denote that impregnation caused a decrease in their values by about 22–37%. Worth noting is also the fact that for all impregnated materials, the values of Rm are about 20% higher. This means that compared to pristine polymers, the carbonisation efficiency of HPP 1 impr, HPP 3 impr, HPP 4 impr, and HPP 6 impr increased by 48.5, 10.1, 12.4, and 37.6%, respectively. Of course, apart from the SA influence, the thermal stability of the precursor itself was also important. For this reason, the highest Rm values were achieved for HPP 3 impr and HPP 4 impr. All these findings allow to prove the protective effect of SA on the surface of the carbonized polymer. During impregnation, aromatic rings of sulphanilic acid created a deposit in porous structure of the precursor. It resulted in not only the formation of very uniform microporosity in the prepared carbons but also delayed and slowed down the process of thermal decomposition of the polymers as well as increased its efficiency.

The synthesized hybrid porous carbons were thermally stable up to 500 °C (Fig. 10 and Table 4). Due to their microporous and hygroscopic nature, in the range of 35–400 °C, a few percent mass change was observed. The level of the obtained value was related not only to the porosity of HPC samples but also to the content of TMVS in the precursor. That is why this effect can be attributed to the hydrophilic properties of silica and silica-derived moieties [70].

Another important feature of silica and silicate species is their high thermal stability [4, 22, 23, 71, 72]. Therefore, the T_{max2} values of HPC 3, HPC 4, and HPC 6 were very similar. Interestingly, the result obtained for HPC 1 was ca. 10 °C higher. Almost identical trend could be observed for decomposition rates. This proved that silica or silicate-like component included in the carbon structure stabilized it, even during the next heating cycles, which is good information from the point of view of potential practical applications. Thermal stability is a very desirable feature, when the material would be used in elevated temperatures, e.g. gas chromatography column packing or thermal regeneration would be applied as a recycling technique.

Evolved gas analysis

More light on the processes taking place during carbonisation threw the evolved gases analysis performed in tandem with TGA. Figure 11 presents Gram Schmidt plots recorded for all the studied samples. Their course allows to compare the gas evolution from the samples as well as makes it easier to indicate at what stage of sample decomposition the infrared spectrum was extracted.

As it was described above, already in the early stages of the process at ca. 300 °C, the HPP 1 sample began to slowly lose its mass. The EGA-FTIR spectra gathered for this polymer and depicted in Fig. 12 showed that ammonia (966 and 930 cm^{-1}) was the first to be released (270–360 °C) from the deamination or condensation of the amide groups. Then at slightly higher temperature, the aliphatic parts of the polymer chains stared to degrade, releasing unsaturated hydrocarbons (3100–2850 cm^{-1}), CO_2 (2360 cm^{-1}), and

Table 4 Thermal parameters of the hybrid porous carbons

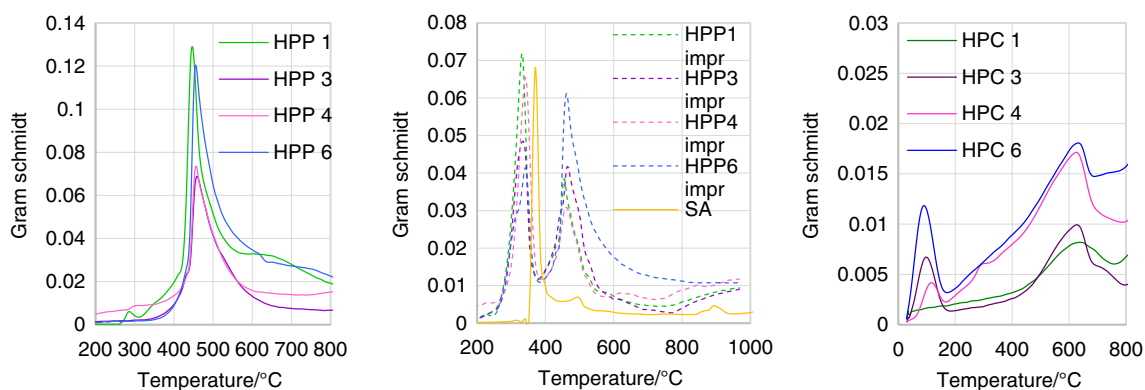|	$T_{5\%}$/°C	$T_{10\%}$/°C	$T_{20\%}$/°C	Δm 35–400 °C/%	Δm 400–1000 °C/%	Rm/%	T_{max1}/°C	Rate of 1st stage/% min^{-1}	T_{max2}/°C	Rate of 2nd stage/% min^{-1}
HPC 1	567.5	664.9	946.5	1.82	19.02	74.02	–	–	663.1	0.60
HPC 3	304.8	672.9	1077.6	4.67	14.16	80.79	94.5	0.54	655.7	0.38
HPC 4	415.1	644.4	1019.2	4.53	17.10	77.98	125.4	0.30	652.7	0.48
HPC 6	112.1	632.0	1020.6	6.18	15.64	77.67	85.2	0.73	653.4	0.41

Fig. 11 The Gram Schmidt curves of the pristine (left), impregnated HPPs (middle), and HPC (right) samples

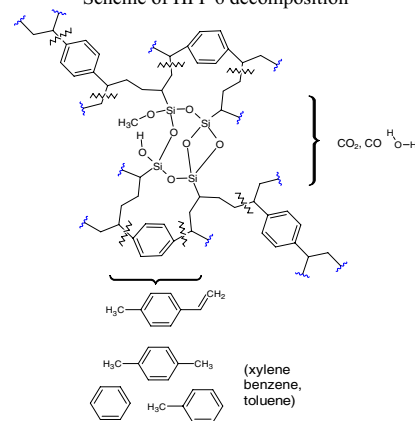**Fig. 12** The EGA-FTIR spectra of HPP 1 and HPP 6 (left) and proposed schemes of their decomposition (right)
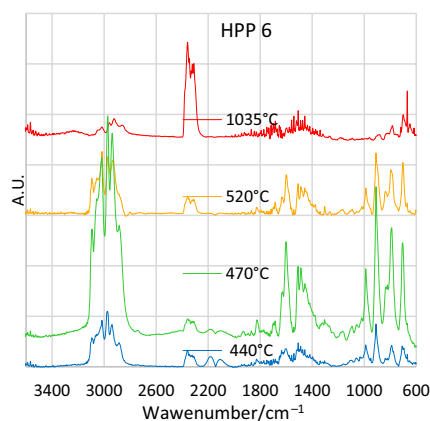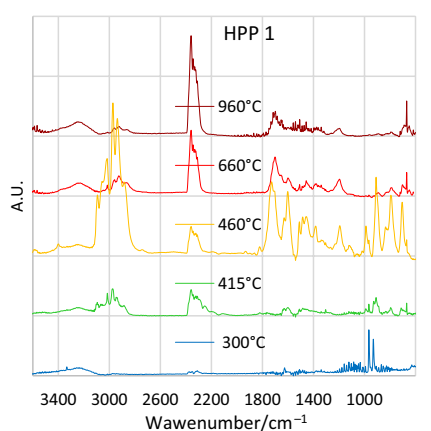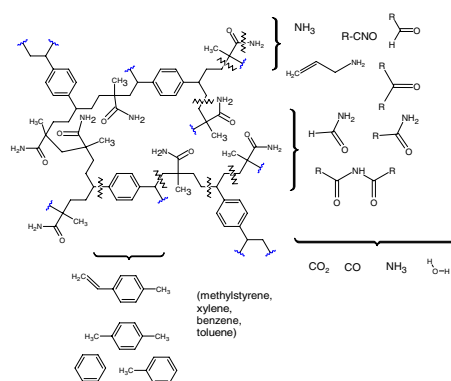
small amounts of nitrile compounds (2250 cm^{-1}), which are characteristic of thermal degradation of acrylamide polymers [34, 35]. At the 460 °C, the released products were dominated by a mixture of aromatic compounds, which indicated further degradation of the polymer, including the cross-linked parts of the chains. The observed characteristic bands could imply the presence m-ethylstyrene (915, 795, 702, 995, and ~3000 cm^{-1} in the range of 300–470 °C), mixture of methylstyrenes (825, 910, and 775 cm^{-1}), styrene (698, 911, 776, and 3095 cm^{-1}), xylenes (798, 731, and 772 cm^{-1}), toluene (731 cm^{-1}), and benzene (672 cm^{-1}), amongst evolved products. The band at 1720 cm^{-1} might disclose the presence of carbonyl derivatives like imides, lactams, aldehydes, and ketones. At 600 °C, thermal decomposition of the polymer is nearly finished. Close to this temperature, reorganisation of charred matter was still taking place. For this reason, amides, imides, unsaturated hydrocarbons (1630 cm^{-1}), and CO_2 were released by the sample.

The same gaseous products were emitted from the sample in the final phase of decomposition at 960 °C, with the difference that CO_2 significantly dominated over the others. The way of releasing all these compounds from the polymer network undergoing disintegration was schematically shown in the right part of Fig. 12, where bond breakage points were marked with zigzag lines.
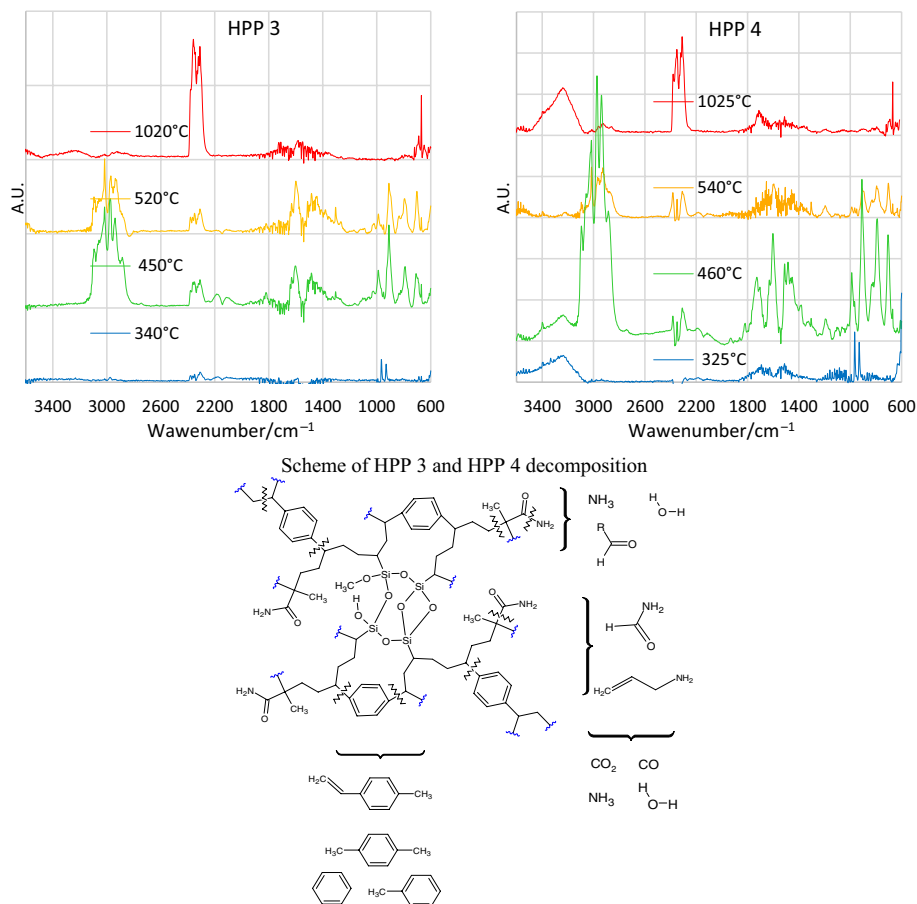
Due to the simpler chemical composition of HPP 6, its thermal destruction also seems to have a much simpler course. In the left bottom panel of Fig. 12, the EGA-FTIR spectra were exhibited, whilst in the right, the suggested degradation scheme for this polymer was exhibited. As follows from the spectrum acquired at 440 °C, the initial step of decomposition concerned free ends of polymer chains. For this reason, in the temperature range of 330–570 °C, m-ethylstyrene dominated in gaseous products, accompanied by small amounts of CO_2 and CO (2170 and 2100 cm^{-1}), and the latter oxides probably came from oxidized fragments of the polymer chains, which could have been formed in a natural way already at the stage of the synthesis. With the rise in temperature (ca. 470 °C), m-ethylstyrene became the main decomposition product suggesting at least partial unzipping mechanism of the process. Such course was already reported for PDVB and PS polymers [73–75]. A further

increase in temperature (ca. 520 °C) caused a change in chemical composition of the released aromatic compounds. Less m-ethylstyrene and more other aromatics (methylstyrenes, styrene, xylenes, and toluene) were emitted from the sample, which was evidenced by changes in the intensities of the characteristic bands from these species observed in the ranges of 3100–2850 cm^{-1} and below 1050 cm^{-1}. Similar to HPP 1, thermal degradation at 600 °C was finished, and further gases were released from residual carbonaceous matter, which consisted partly of the carbonized polymer and partly of silica/silicate derivatives. At 1035 °C, mainly CO_2 and small quantities of H_2O (1300–2000 and above 3500 cm^{-1}) and simple aromatic hydrocarbons like benzene, toluene, or xylenes were evolved as the last decomposition products.

In case of the HPP 4 terpolymer (Fig. 13), the decomposition runs in the similar way as for HPP 1. The same products were released at relevant stages of the process in proportions corresponding to the chemical composition of the polymeric precursor. At about 325 °C, ammonia, then aromatic compounds in the range of 320–630 °C, and at the end of the analysis, mostly CO_2 and H_2O (1025 °C) were identified in the released gaseous products.

Although HPP 3 only slightly differed from HPP 4 in chemical composition, its thermal behaviour was more

Fig. 13 The EGA-FTIR spectra of HPP 3 and HPP 4 (on top) and suggested schemes of their decomposition (bottom)

similar to HPP 6. Up to 350 °C, it gave off hardly any gases besides ammonia. Then from the beginning of thermal decomposition to achieving T_{max2}, mostly m-ethylstyrene (330–560 °C), CO_2, and CO were evolved. As the reaction proceeded (520 °C), other aromatic compounds also appeared in the decomposition products. Finally, CO_2 and H_2O predominated in the emitted gases.

Before starting considerations on the influence of sulphanilic acid on the carbonisation process of impregnated polymers, it is worth looking into its own decomposition. In the upper panel of Fig. 14, the EGA-FTIR spectra of SA and a simplified diagram of the process are presented. The thermal degradation of surface modifier started at about 300 °C. Initially (80–350 °C), only H_2O was evolved proving that SA forms a monohydrate. When at ca. 380 °C, the release of water was almost over, and SO_2 (1372, 1163, and 1137 cm^{-1}) and a little amount of CO_2 appeared in the decomposition products, indicating that the process began

Fig. 14 The EGA-FTIR spectra of sulphanilic acid and impregnated hybrid polymer precursors. At upper right corner, scheme of possible thermal degradation of SA was added

with the cleavage of the sulfone group accompanied by oxidation of decomposition products. The SO_2 emission proceeded in the temperature range of 340–420 °C. Next, at higher temperature (400–550 °C), mainly aniline (3037, 1610, 1490, 1277, 753, and 690 cm^{-1}) was released. Finally, small amounts of CO_2, CO, and sulphonamide derivatives (3390–3245 and ca. 1600 cm^{-1}) were observed in the spectrum of final products of residual matter decomposition.

After impregnation, decomposition ran in two stages. It could suggest that one step should correspond to the degradation of the modifier and the other to the polymer, but this is not the case. From Fig. 14, it follows that thermal destruction of HPP 1 impr started with releasing of ammonia in the same way as for HPP 1. However, the temperature range was broader (220–420 °C). At similar range (230–420 °C), SO_2 was evolved, as well. That was approximately 120 °C lower compared to pure SA. The same also applied to aniline release, and its emission occurred from 310 to 490 °C. These observations confirmed the earlier thesis about decomposition of SA at a lower temperature, due to its inability to create a crystal structure in the polymer pores. Other aromatic compounds, characteristic of polymer destruction, were detected in the temperature range of 390–570 °C, which in turn was higher than for HPP 1, confirming the validity of the assumption about the protective effect of SA on the polymer surface.

In the case of HPP 6 impr, SO_2 was released from 200 to 400 °C, which was even lower than for HPP 1 impr. This can be due to the better developed porosity of the polymer, especially in the micropore range. Aniline was evolved from 360 to 490 °C; thus, its temperature range shifted 40° down in comparison with SA. The emission of m-ethylstyrene took place from 350 to 610 °C which was 20° higher than for HPP 6. Other aromatic compounds were given off in a broad range of temperature due to the complex course of thermal decomposition. The analysis of EGA-FTIR spectra proved the protective influence of SA on this material, as well.

The same protective effect was observed for the next two polymers, HPP 3 impr and HPP 4 impr. Up to 200 °C, besides releasing some H_2O, and in case of HPP 3 impr, also CH_3OH (1070, 3000 and 12,445 cm^{-1}) took place. Their amount was about 1.5% according to TG analyses. The presence of water resulted both from the hygroscopic properties of SA and from the polymers nature, which favours the adsorption of steam from the air around their hydrophilic functional groups, whilst methanol was probably a residue trapped in the porous structure of the polymer during washing in a Soxhlet apparatus. At higher temperature (220–400 °C), both materials evolved ammonia. Emission of SO_2 was observed in the range of 210–400 °C for the HPP 3 impr sample and 230–410 °C for HPP 4 impr, revealing their similarities to HPP 6 impr and HPP 1 impr,

respectively, especially in terms of porosity. On the other hand, aniline was released by both impregnated polymers in the temperature range of 340–500 °C, which was intermediate compared to HPP 1 impr and HPP 6 impr, giving off m-ethylstyrene for both materials started at 340 °C. However, in case HPP 3 impr, the end of the process took place at 640 °C, whilst for HPP 4 impr, it lasted up to 690 °C. The obtained values were higher than those of the pristine precursors (HPP 3 and HPP 4) by 80 and 60 °C, respectively.

At the final stage of decomposition, above 600 °C, methane, CO, and increasing amounts of CO_2 were given off by the HPP 1 impr, HPP 3 impr, and HPP 4 impr samples. This observation suggested that at this stage, the MA-containing polymers were already carbonized and further structural changes resulted from the internal transformation of this newly formed charred matter. Comparing these results with the results obtained for the pristine precursors, it should be noted that there was no methane in the decomposition products of the latter. This observation led to a conclusion that sulphanilic acid contributed to the formation of both the porous structure and the chemical heterogeneity of the surface of carbonized products.

Figure 15 presents the EGA-FTIR spectra of hybrid porous carbons. Due to the hydrophilic surface properties and the developed microporous structure, the HPC samples retained some water and/or acetone, which were used to rinse the materials after carbonisation. Its emission took place up to 200 °C.

At higher temperature, in the decomposition products of the hybrid carbons, mostly H_2O, CO_2, CO, and CH_4 were found. The scheme in Fig. 14 shows the way of formation of such compounds. Their presence at particular stages of thermal degradation depends on the chemical structure of a carbon [76, 77]. Functional groups on the surface of carbonized materials are formed from precursor under definite carbonisation conditions. In these studies, thermal treatment of the hybrid polymers was carried out according to the same procedure that allowed to show differences resulting from various chemical structures of precursors. The comparison of the temperature ranges of above-mentioned products released by HPC materials is depicted in Table 5.

From this table, it follows that surface functional groups of HPC can include carboxyl (H_2O, CO_2), carboxylic anhydride (CO_2, CO), ether, carbonyl, or quinone (CO) and phenol (H_2O, CO) moieties. The presence of methane and unsaturated hydrocarbons resulted from further decomposition of the carbonized matter. The amine derivatives were residues of MA, but they could also be formed by the interaction of SA with the heat-treated surface of the impregnated precursors.

Fig. 15 The EGA-FTIR spectra of HPC samples and possible schemes of their decomposition (at the bottom)
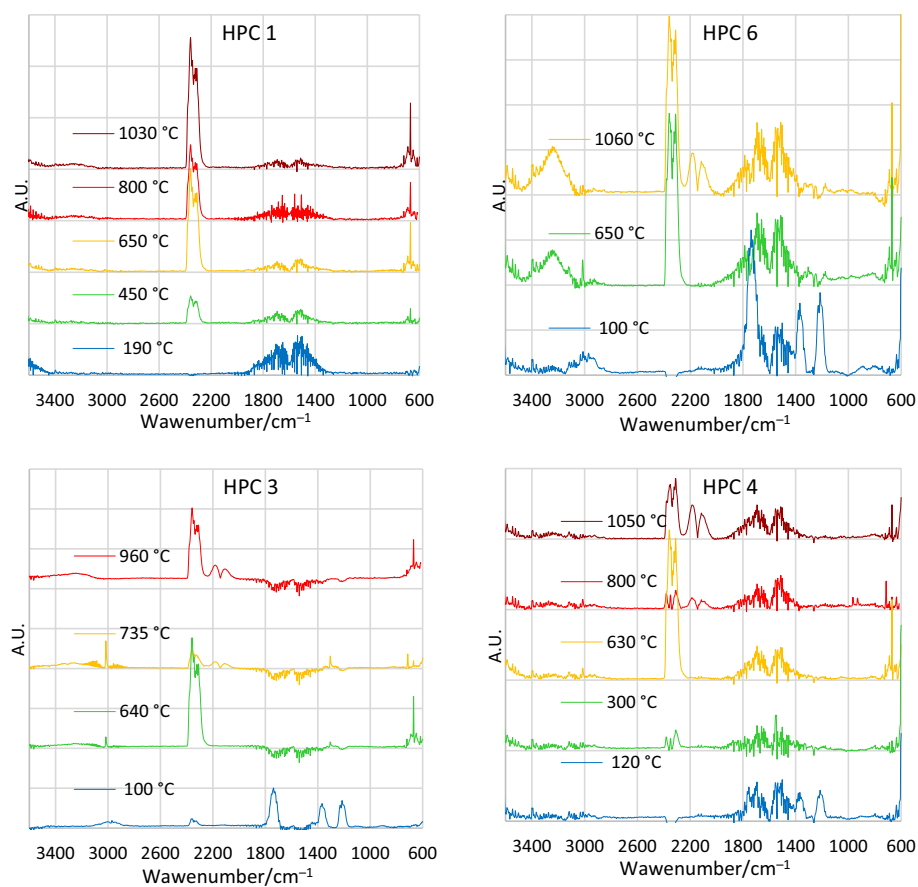
Scheme of HPCs decomposition
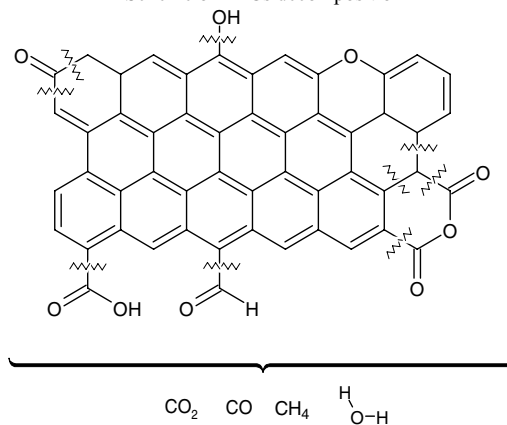
Table 5 The temperature ranges of products evolved from HPC samples

	HPC 1	HPC 4	HPC 3	HPC 6
CO_2 (2360 cm^{-1})	290–780	290–350; 400–730	370–790	390–710
CO (2170 cm^{-1})	–	640–800	650–780	650–780
H_2O (3500 cm^{-1})	Full range	30–800	–	Full range
CH_4 (3016; 1305 cm^{-1})	–	550–830	560–840	580–850
Unsaturated hydrocarbons (653 cm^{-1})	320–700	270–780	150–800	440–720
Secondary amines (714 cm^{-1})	522–815	640–900	650–830	660–850

Conclusions

The TGA-EGA technique was used in this work to evaluate the influence of sulphanilic acid on the carbonisation process of the hybrid polymeric precursors. The research was carried out by comparing the data obtained for the pristine and the impregnated precursors with those for carbons prepared by thermal treatment of impregnated precursors. The chemical structure of pristine hybrid polymers and the resulting carbons were characterized by FTIR, Raman, and PXRD spectroscopic methods. The performed studies revealed the presence of amorphous phase composed of the polymer chains or the small fragments of carbon interpenetrated by silica/silicate disordered network.

The first effect of sulphanilic acid on the properties of the obtained hybrid porous carbons was proven by porosimetric analysis. The resulted carbons showed a significant development of homogeneous micropores with the average pore width of 0.7 nm and reduced number of mesopores compared to pristine precursors.

Further effects of using sulphanilic acid were revealed by thermogravimetric analysis. The main findings resulting from the comparison of the TG data for pristine and impregnated polymers were as follows:

- the reduction of the IDT of impregnated polymers by about 100 °C;
- the increase in their T_{max} by 2–5.5 °C;
- slowing down the rate of carbonisation process by 22–37%;
- slight extending of the range of decomposition temperature;
- the increase in efficiency of the carbonisation by 10–48%.

These observations led to the conclusion that SA had the protective effect on the surface of the carbonized polymers. During impregnation and thermal treatment, the aromatic rings of sulphanilic acid produced a deposit in porous structure of the precursors. As a consequence, not only uniform microporous structure was created, but also this layer acted as a surface protection, which delayed and slowed down the process of the polymer thermal decomposition and increased its efficiency. A detailed FTIR analysis of evolved gases confirmed the above-described mechanism of action of sulphanilic acid and additionally proved its influence on the chemical heterogeneity of the surface of the prepared hybrid porous carbons.

Declarations

References

1. Kango S, Kalia S, Celli A, Njuguna J, Habibi Y, Kumar R. Surface modification of inorganic nanoparticles for development of organic–inorganic nanocomposites—a review. Prog Polym Sci. 2013;38:1232–61.
2. Tiwari I, Mahanwar PA. Polyacrylate/silica hybrid materials: a step towards multifunctional properties. J Dispers Sci Technol. 2019;40:925–57. https://doi.org/10.1080/01932691.2018.1489276.
3. Gómez-Romero P, Gomez-Romero BP. Hybrid organic-inorganic materials—in search of synergic activity. Adv Mater. 2001;13:163–74.
4. Niemczyk A, Dziubek K, Sacher-Majewska B, Czaja K, Czech-Polak J, Oliwa R, et al. Thermal stability and flame retardancy of polypropylene composites containing siloxane-silsesquioxane resins. Polymers (Basel). 2018;10:1019.
5. Klepka T, Podkościelna B, Czerwiński D, Samujło B. The influence of silica nanoparticles on the thermal and mechanical properties of crosslinked hybrid composites. Materials (Basel). 2021;14:7431.
6. Pierre AC, Pajonk GM. Chemistry of aerogels and their applications. Chem Rev. 2002;102:4243–65.
7. Podkościelna B, Sobiesiak M. Synthesis and characterization of organic–inorganic hybrid microspheres. Adsorption. 2016;22:631–8. https://doi.org/10.1007/s10450-015-9741-1.
8. Goliszek M, Sobiesiak M, Fila K, Podkościelna B. Evaluation of sorption capabilities of biopolymeric microspheres by the solid-phase extraction. Adsorption. 2019;25:289–300. https://doi.org/10.1007/s10450-019-00008-6.
9. Wu T, Ke Q, Lu M, Pan P, Zhou Y, Gu Z, et al. Recent advances in carbon-silica composites: preparation, properties, and applications. Catalysts. 2022;12:573.
10. Inagaki M, Kang F. Fundamental science of carbon materials. In: Materials science and engineering of carbon: fundamentals. Elsevier; 2014. pp. 17–217.
11. Wang H, Shao Y, Mei S, Lu Y, Zhang M, Sun J, et al. Polymer-derived heteroatom-doped porous carbon materials. Chem Rev.

2020;120:9363–419. https://doi.org/10.1021/acs.chemrev.0c000 80.

12. Simonsen ME, Sønderby C, Li Z, Søgaard EG. XPS and FT-IR investigation of silicate polymers. J Mater Sci. 2009;44:2079–88. https://doi.org/10.1007/s10853-009-3270-9.

13. Ahangaran F, Navarchian AH. Recent advances in chemical surface modification of metal oxide nanoparticles with silane coupling agents: a review. Adv Colloid Interface Sci. 2020;286:102298. https://doi.org/10.1016/j.cis.2020.102298.

14. Giasuddin ABM, Cartwright A, Britt DW. Silica nanoparticles synthesized from 3,3,3-Propyl(trifluoro)trimethoxysilane or n -Propyltrimethoxysilane for creating superhydrophobic surfaces. ACS Appl Nano Mater. 2021;4:4092–102. https://doi.org/10.1021/acsanm.1c00398.

15. Rios X, Moriones P, Echeverría JC, Luquin A, Laguna M, Garrido JJ. Ethyl group as matrix modifier and inducer of ordered domains in hybrid xerogels synthesised in acidic media using ethyltriethoxysilane (ETEOS) and tetraethoxysilane (TEOS) as precursors. Mater Chem Phys. 2013;141:166–74. https://doi.org/10.1016/j.matchemphys.2013.04.042.

16. Pielichowski K, Njuguna J, Janowski B, Pielichowski J. Polyhedral oligomeric silsesquioxanes (POSS)-containing nanohybrid polymers. Adv Polym Sci. 2006. https://doi.org/10.1007/12_077.

17. Laine RM. Nanobuilding blocks based on the [OSiO1.5]x (×=6, 8, 10) octasilsesquioxanes. J Mater Chem. 2005;15:3725.

18. Shimojima A, Kuroda K. Alkoxy- and silanol-functionalized cage-type oligosiloxanes as molecular building blocks to construct nanoporous materials. Molecules. 2020;25:524.

19. Wan Y, Shi Y, Zhao D. Supramolecular aggregates as templates: ordered mesoporous polymers and carbons†. Chem Mater. 2008;20:932–45. https://doi.org/10.1021/cm7024125.

20. Huang J, He C, Xiao Y, Mya KY, Dai J, Siow YP. Polyimide/POSS nanocomposites: interfacial interaction, thermal properties and mechanical properties. Polymer (Guildf). 2003;44:4491–9.

21. Mantz RA, Jones PF, Chaffee KP, Lichtenhan JD, Gilman JW, Ismail IMK, et al. Thermolysis of polyhedral oligomeric silsesquioxane (POSS) macromers and POSS−siloxane copolymers. Chem Mater. 1996;8:1250–9. https://doi.org/10.1021/cm950536x.

22. Blanco I, Abate L, Bottino FA. Synthesis and thermal properties of new dumbbell-shaped isobutyl-substituted POSSs linked by aliphatic bridges. J Therm Anal Calorim. 2014;116:5–13.

23. Liu YR, Huang YD, Liu L. Thermal stability of POSS/methylsilicone nanocomposites. Compos Sci Technol. 2007;67:2864–76.

24. Jang BN, Costache M, Wilkie CA. The relationship between thermal degradation behavior of polymer and the fire retardancy of polymer/clay nanocomposites. Polymer (Guildf). 2005;46:10678–87.

25. Herrera M, Wilhelm M, Matuschek G, Kettrup A. Thermoanalytical and pyrolysis studies of nitrogen containing polymers. J Anal Appl Pyrolysis. 2001;58–59:173–88.

26. Zuo M, Takeichi T, Matsumoto A, Tsutsumi K. Surface characterization of polyimide films. Colloid Polym Sci. 1998;276:555–64. https://doi.org/10.1007/s003960050281.

27. Zhang B, Jiang Y, Balasubramanian R. Synthesis, formation mechanisms and applications of biomass-derived carbonaceous materials: a critical review. J Mater Chem A. 2021;9:24759–802.

28. Kiciński W, Dyjak S. Nitrogen-doped carbons derived from imidazole-based cross-linked porous organic polymers. Molecules. 2021;26:668.

29. Pels J, Kapteijn F, Moulijn J, Zhu Q, Thomas K. Evolution of nitrogen functionalities in carbonaceous materials during pyrolysis. Carbon N Y. 1995;33:1641–53.

30. Huang C, Puziy AM, Poddubnaya OI, Hulicova-Jurcakova D, Sobiesiak M, Gawdzik B. Phosphorus, nitrogen and oxygen co-doped polymer-based core-shell carbon sphere for high-performance hybrid supercapacitors. Electrochim Acta. 2018;270:339–51.

31. Kapteijn F, Moulijn JA, Matzner S, Boehm H-P. The development of nitrogen functionality in model chars during gasification in CO₂ and O₂. Carbon N Y. 1999;37:1143–50.

32. Ayiania M, Smith M, Hensley AJR, Scudiero L, McEwen J-S, Garcia-Perez M. Deconvoluting the XPS spectra for nitrogen-doped chars: an analysis from first principles. Carbon N Y. 2020;162:528–44.

33. Chen W, Yang H, Chen Y, Chen X, Fang Y, Chen H. Biomass pyrolysis for nitrogen-containing liquid chemicals and nitrogen-doped carbon materials. J Anal Appl Pyrolysis. 2016;120:186–93.

34. Van Dyke JD, Kasperski KL. Thermogravimetric study of polyacrylamide with evolved gas analysis. J Polym Sci Part A Polym Chem. 1993;31:1807–23. https://doi.org/10.1002/pola.1993.080310720.

35. Grassie N, McNeill IC, Samson JNR. The thermal degradation of polymethacrylamide and copolymers of methacrylamide and methyl methacrylate. Eur Polym J. 1978;14:931–7.

36. Kim S, Seo M. Control of porosity in hierarchically porous polymers derived from hyper-crosslinked block polymer precursors. J Polym Sci Part A Polym Chem. 2018;56:900–13. https://doi.org/10.1002/pola.28966.

37. Sobiesiak M. New bio-based polymer sorbents out of terpene compounds or vegetable oils: synthesis, properties, analysis of sorption processes. Polymers (Basel). 2022;14:5389.

38. Maciejewska M. Characterization of thermal properties of porous microspheres bearing pyrrolidone units. J Therm Anal Calorim. 2015;119:1147–55.

39. Silverstein MS. The chemistry of porous polymers: the holey grail. Isr J Chem. 2020;60:140–50. https://doi.org/10.1002/ijch.20200 0003.

40. Jedynak K, Charmas B. Preparation and characterization of physicochemical properties of spruce cone biochars activated by CO₂. Materials (Basel). 2021;14:3859.

41. Sobiesiak M. Nanoporous carbons obtained by carbonization of copolymers impregnated by salts. Adsorption. 2012;19:349–56. https://doi.org/10.1007/s10450-012-9457-4.

42. Kawabuchi Y, Kishino M, Kawano S, Whitehurst DD, Mochida I. Carbon deposition from benzene and cyclohexane onto active carbon fiber to control its pore size. Langmuir. 1996;12:4281–5. https://doi.org/10.1021/la960292a.

43. Kawabuchi Y, Sotowa C, Kuroda K, Kawano S, Whitehurst DD, Mochida I. Chemical vapor deposition of organic compounds over active carbon fiber to control its porosity and surface function. ACS Symp Ser. 1997. https://doi.org/10.1021/bk-1998-0681.ch007.

44. Kyotani T. Control of pore structure in carbon. Carbon N Y. 2000;38:269–86.

45. Moreira RFP, José H, Rodrigues A. Modification of pore size in activated carbon by polymer deposition and its effects on molecular sieve selectivity. Carbon N Y. 2001;39:2269–76.

46. Sobiesiak M. Thermal properties of nanoporous carbons prepared by a template method using different polymeric and organic precursors. New Carbon Mater. 2012;27:337–43.

47. Choma J, Jedynak K, Marszewski M, Jaroniec M. Polymer-templated mesoporous carbons synthesized in the presence of nickel nanoparticles, nickel oxide nanoparticles, and nickel nitrate. Appl Surf Sci. 2012;258:3763–70.

48. Puziy AM, Poddubnaya OI, Gawdzik B, Sobiesiak M, Reinish CA, Tsyba MM, et al. Nanostructured carbons for solid phase extraction. Appl Surf Sci. 2010;256:5216–20.

49. Libbrecht W, Verberckmoes A, Thybaut JW, Van Der Voort P, De Clercq J. Soft templated mesoporous carbons: tuning the porosity for the adsorption of large organic pollutants. Carbon N Y. 2017;116:528–46. https://doi.org/10.1016/j.carbon.2017.02.016.

50. Schlumberger C, Thommes M. Characterization of hierarchically ordered porous materials by physisorption and mercury porosimetry—a tutorial review. Adv Mater Interfaces. 2021. https://doi.org/10.1002/admi.202002181.

51. Cychosz KA, Guillet-Nicolas R, García-Martínez J, Thommes M. Recent advances in the textural characterization of hierarchically structured nanoporous materials. Chem Soc Rev. 2017;46:389–414.

52. Podkościelna B, Fila K, Gil M, Nowak J. Synthesis and characterization of new hybrid microspheres with amide functionalization. Adsorpt Sci Technol. 2017;35:422–31. https://doi.org/10.1177/0263617417694364.

53. Simonsen ME, Sønderby C, Li Z, Søgaard EG. XPS and FT-IR investigation of silicate polymers. J Mater Sci. 2009;44:2079–88.

54. Park ES, Ro HW, Nguyen CV, Jaffe RL, Yoon DY. Infrared spectroscopy study of microstructures of poly (silsesquioxane)s. Chem Mater. 2008;20:1548–54.

55. Socrates G. Infrared and Raman Frequencies Characteristic Group. 3rd ed. George Socrates, The University of West London, Middlesex UK, editor. Chichester: John Wiley & Sons LTD; 2001.

56. Smith MW, Dallmeyer I, Johnson TJ, Brauer CS, McEwen JS, Espinal JF, et al. Structural analysis of char by Raman spectroscopy: Improving band assignments through computational calculations from first principles. Carbon N Y. 2016;100:678–92. https://doi.org/10.1016/j.carbon.2016.01.031.

57. Sadezky A, Muckenhuber H, Grothe H, Niessner R, Pöschl U. Raman microspectroscopy of soot and related carbonaceous materials: spectral analysis and structural information. Carbon N Y. 2005;43:1731–42.

58. Ahmed MA, Khafagy RM, Bishay ST, Saleh NM. Effective dye removal and water purification using the electric and magnetic Zn0.5Co0.5Al0.5Fe1.46La0.04O4/polymer core–shell nanocomposites. J Alloys Compd. 2013;578:121–31.

59. Haward RN, editor. The physics of glassy polymers. 1st ed. Dordrecht: Springer; 1973.

60. Niculăescu C, Olar L, Stefan R, Todica M, Pop CV. XRD and IR investigations of some commercial polystyrene samples thermally degraded. Stud Univ Babeș-Bolyai Chem. 2018;63:63–70.

61. Fan L, Fukada T, Annaka M, Yoshikuni M, Nakahira T. Secondary structure and side-chain chromophore orientation of isotactic poly(methacrylamide)s in solid film. Polym J. 1999;31:364–8. https://doi.org/10.1295/polymj.31.364.

62. Yemata TA, Zheng Y, Kyaw AKK, Wang X, Song J, Chin WS, et al. Improved thermoelectric properties and environmental stability of conducting PEDOT:PSS films post-treated with imidazolium ionic liquids. Front Chem. 2020;7:1–16. https://doi.org/10.3389/fchem.2019.00870/full.

63. Hung C-H, Singh B, Landowski MG, Ibrahim M, Miles AJ, Jensen DS, et al. Multi-instrument characterization of poly(divinylbenzene) microspheres for use in liquid chromatography: as received, air oxidized, carbonized, and acid treated. Surf Interface Anal. 2015;47:815–23. https://doi.org/10.1002/sia.5778.

64. Rao Penki T, N. Munichandraiah B, Shanmughasundaram D. High rate capability of coconut kernel derived carbon as an anode material for lithium-ion batteries. Adv Mater Lett. 2014;5:184–90.

65. Zickler GA, Smarsly B, Gierlinger N, Peterlik H, Paris O. A reconsideration of the relationship between the crystallite size La of carbons determined by X-ray diffraction and Raman spectroscopy. Carbon N Y. 2006;44:3239–46.

66. Puech P, Dabrowska A, Ratel-Ramond N, Vignoles GL, Monthioux M. New insight on carbonisation and graphitisation mechanisms as obtained from a bottom-up analytical approach of X-ray diffraction patterns. Carbon N Y. 2019;147:602–11.

67. Putman KJ, Rowles MR, Marks NA, de Tomas C, Martin JW, Suarez-Martinez I. Defining graphenic crystallites in disordered carbon: moving beyond the platelet model. Carbon N Y. 2023;209:117965. https://doi.org/10.1016/j.carbon.2023.03.040.

68. Mubari PK, Beguerie T, Monthioux M, Weiss-Hortala E, Nzihou A, Puech P. The X-ray, Raman and TEM signatures of cellulose-derived carbons explained. C. 2022;8:4.

69. Low JN, Glidewell C. A quasi-diamondoid hydrogen-bonded framework in anhydrous sulfanilic acid. Acta Crystallogr Sect C Cryst Struct Commun. 2002;58:o209–11.

70. Ng E-P, Mintova S. Nanoporous materials with enhanced hydrophilicity and high water sorption capacity. Microporous Mesoporous Mater. 2008;114:1–26.

71. Meier D, Huch V, Kickelbick G. Aryl-group substituted polysiloxanes with high-optical transmission, thermal stability, and refractive index. J Polym Sci. 2021;59:2265–83. https://doi.org/10.1002/pol.20210316.

72. Sahiner N, Sagbas S, Aktas N. Preparation and characterization of monodisperse, mesoporous natural poly(tannic acid)-silica nanoparticle composites with antioxidant properties. Microporous Mesoporous Mater. 2016;226:316–24. https://doi.org/10.1016/j.micromeso.2016.02.012.

73. Li Y, Fan Y, Ma J. The thermal properties of porous polydivinylbenzene beads. React Funct Polym. 2002;50:57–65.

74. Beyler CL, Hirschler MM. Thermal decomposition of polymers. SFPE Handbook of Fire Protection Engineering 2, Section 1, Chapter 7, 2002.

75. Levchik GF, Si K, Levchik SV, Camino G, Wilkie CA. The correlation between cross-linking and thermal stability: cross-linked polystyrenes and polymethacrylates. Polym Degrad Stab. 1999;65:395–403.

76. Stein A, Wang Z, Fierke MA. Functionalization of porous carbon materials with designed pore architecture. Adv Mater. 2009;21:265–93. https://doi.org/10.1002/adma.200801492.

77. Rocha RP, Pereira MFR, Figueiredo JL. Characterisation of the surface chemistry of carbon materials by temperature-programmed desorption: an assessment. Catal Today. 2023. https://doi.org/10.1016/j.cattod.2023.114136.